AIChE WILEY InterScience DISCOVER SOMETHING GREAT



# Mechanistic Study of Enhanced $H_2$ Synthesis in Biomass Gasifiers with In-Situ $CO_2$ Capture Using CaO

**Nicholas H. Florin and Andrew T. Harris**
Laboratory for Sustainable Technology, School of Chemical and Biomolecular Engineering, University of Sydney, NSW 2006, Australia

*DOI 10.1002/aic.11434*
*Published online February 19, 2008 in Wiley InterScience (www.interscience.wiley.com).*

*Biomass gasification coupled with in situ $CO_2$ removal using CaO is a promising process for the sustainable production of $H_2$. Thermodynamic equilibrium modeling predicts biomass conversion to gas containing up to 81.4 vol % $H_2$ (dry basis). However, in practice, discrepancies between theoretical and experimental results demonstrate the significance of nonequilibrium phenomena. In this context, we have developed a simultaneous thermogravimetric-mass spectrometric (TG-MS) technique to study the influence of: (i) heating rate, (ii) CaO loading, (iii) evolved gas residence time, and (iv) reaction atmosphere. The results of this study give insight into the decomposition mechanisms of biomass in the presence of CaO, including the influence of: (i) $CO_2$ removal, (ii) sorbent hydration ($Ca(OH)_2$), (iii) intrinsic heating and swelling effects associated with the exothermic gas–solid absorption reactions, and (iv) the direct catalytic role of CaO for char gasification and tar elimination.*  *AIChE J*, 54: 1096–1109, 2008
*Keywords: $CO_2$ capture, carbonation, cellulose pyrolysis, hydrogen*

## Introduction

The generation of energy from biomass is relevant in light of concerns regarding local energy security and the urgent need to mitigate greenhouse gas emissions.[1] Biomass has been widely acknowledged as a key resource for meeting future energy demand in both the developed and the majority world.[2]

A promising way to exploit biomass resources for energy and fuel production involves converting biomass into a $H_2$-rich synthesis gas. $H_2$ production from biomass would help to secure local energy supply because of the diversity and abundance of biomass resources. Theoretically, $H_2$ produced from biomass can be $CO_2$ neutral because the equivalent quantity of $CO_2$ evolved during biomass conversion is removed from the atmosphere via photosynthesis. Furthermore, the coupling of biomass conversion technologies with $CO_2$ capture and storage technologies offers the potential to achieve a reduction in $CO_2$ from the atmosphere.

First, this article demonstrates the merits of a combined biomass gasification/$CO_2$ removal process on the basis of thermodynamic equilibrium modeling and previous experimental studies. In this context, we present experimental results providing insight into the important (nonequilibrium) mechanistic pathways underpinning the enhanced synthesis of $H_2$ in biomass gasifiers combined with in-situ $CO_2$ removal using CaO.

### *Enhanced $H_2$ synthesis in biomass gasifiers*

An outline of the conversion process for biomass gasification is given in Figure 1. This process involves three main steps, which is defined by reaction temperature.[3–5] (i) Pyrolysis (573–773 K), (ii) cracking and reforming reactions (greater than 773 K), and (iii) char gasification reactions (typically greater than 1073 K). Because biomass fuels usu-

Correspondence concerning this article should be addressed to Nicholas H. Florin at n.florin@usyd.edu.au.

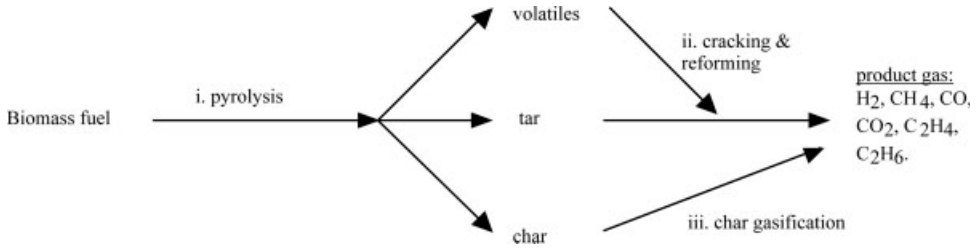


**Figure 1. Simplified reaction mechanism for the gasification of biomass fuels: after Higman and van der Burgt[5]).**

ally consist of 70–90 wt % volatiles, the pyrolysis and secondary cracking and reforming reactions (i.e. steps i and ii) are particularly important for determining the final product distribution.[3,5]

In a biomass gasifier these steps occur simultaneously due to moderate/high heating rates. Therefore, the overall process may be summarized by a series of competing reactions involving heterogeneous interactions between evolved gas species and the decomposing solid residue and homogeneous interactions between the evolved gas species, steam, and interactions among evolved gas species. The important reactions are presented in Table 1. The relative dominance of these interactions for determining the distribution of products, i.e. gas, tar, and char yields, is dependent on the gasifier design and the operating conditions. Thus, understanding the effect of the key operating parameters is necessary in order to manipulate the distribution of the products for maximizing the output of $H_2$.

The $H_2$ concentration in the product gas from biomass gasification without $CO_2$ removal is typically only 40–50 vol %.[4,7–11] To enhance the $H_2$ concentration, the process can be combined with in-situ $CO_2$ removal using CaO. The fundamental idea is that the removal of $CO_2$, as soon as it is formed, shifts the conversion process beyond equilibrium limitations, e.g. according to Eq. 1. $CO_2$ removal with CaO occurs according to Eq. 13.

Carbonation:

$$CaO + CO_2 \rightarrow CaCO_3 \quad \Delta H^0_{873.15} = -171.2\,\text{kJ/mol} \qquad (13)$$

In addition to the primary function of CaO for $CO_2$ capture, the catalytic role of CaO for tar decomposition is well known, although the mechanism is not understood.[12,13] Improved tar destruction is expected to further enhance the $H_2$ output, according to Eqs. 3–6.

When CaO is fully converted to $CaCO_3$, it can be regenerated by reversing the capture reaction, according to Eq. 14. Regeneration is achieved by heating $CaCO_3$ to 973–1223 K, depending on the $CO_2$ partial pressure. High calcination temperatures are required in order to produce a pure stream of $CO_2$ suitable for sequestration technologies.[14]

Calcination:

$$CaCO_3 \rightarrow CaO + CO_2 \quad \Delta H^0_{873.15} = -171.2\,\text{kJ/mol} \qquad (14)$$

The likely configuration for this coupled gasification/$CO_2$ removal process involves operating a gasifier in parallel with a regeneration reactor.[15–17] Biomass fuel is continuously fed to the gasifier and sorbent material is circulated from the gasifier in the form of $CaCO_3$ to the regenerator and from the regenerator in the form of CaO back to the gasifier. The delivery of the hot CaO to the gasifier provides additional heat for the endothermic cracking and reforming reactions, Eqs. 2–11.[16,17]

### *Implications of thermodynamic equilibrium*

Enhanced $H_2$ synthesis in biomass gasifiers with $CO_2$ removal using CaO can be easily demonstrated based on thermodynamic equilibrium theory.

In this article, we present thermodynamic equilibrium modeling predictions to provide a useful basis for understanding the decomposition data presented in "Results and Discussion." A more detailed study is published elsewhere.[18]

**Table 1. Important Chemical Reactions for Steam Gasification of Biomass Fuels[3–7]**

| Name of Reaction | Chemical Equation | $\Delta H^0_{873.15}$ (KJ/mol) | Equation Number |
|---|---|---|---|
| Water–gas shift | $CO + H_2O \rightarrow CO_2 + H_2$ | −36.1, Exothermic | 1 |
| Steam reforming (i) | $CH_4 + H_2O \rightarrow CO + 3H_2$ | 224.1, Endothermic | 2 |
| Steam reforming (ii) | $C_nH_m{}^* + nH_2O \rightarrow nCO + (n + m/2)H_2$ | Endothermic | 3 |
| Dry reforming | $C_nH_m + nCO_2 \rightarrow 2nCO + (m/2)H_2$ | Endothermic | 4 |
| Hydrocracking | $C_nH_m + H_2 \rightarrow C_{n-x}H_{m-y} + \cdots + H_2$, $CH_4 + \cdots + C$ | Endothermic | 5 |
| Thermal cracking | $C_nH_m \rightarrow C_{n-x}H_{m-y}{}^{**} + \cdots + H_2$, $CH_4 + \cdots + C$ | Endothermic | 6 |
| Water–gas (i) | $C + H_2O \rightarrow CO + H_2$ | 135.7, Endothermic | 7 |
| Water–gas (ii) | $C + 2H_2O \rightarrow CO_2 + 2H_2$ | 99.7, Endothermic | 8 |
| Oxidation (i) | $C + O_2 \rightarrow CO_2$ | −394.3, Exothermic | 9 |
| Oxidation (ii) | $C + 0.5O_2 \rightarrow CO$ | −111.3, Exothermic | 10 |
| Boudouard | $C + CO_2 \rightarrow 2CO$ | 171.8, Endothermic | 11 |
| Methanation | $C + 2H_2 \rightarrow CH_4$ | −88.3, Exothermic | 12 |

*$C_nH_m$ represents tar species.
**$C_{n-x}H_{m-y}$ represents tar species subsequent to a primary decomposition step.

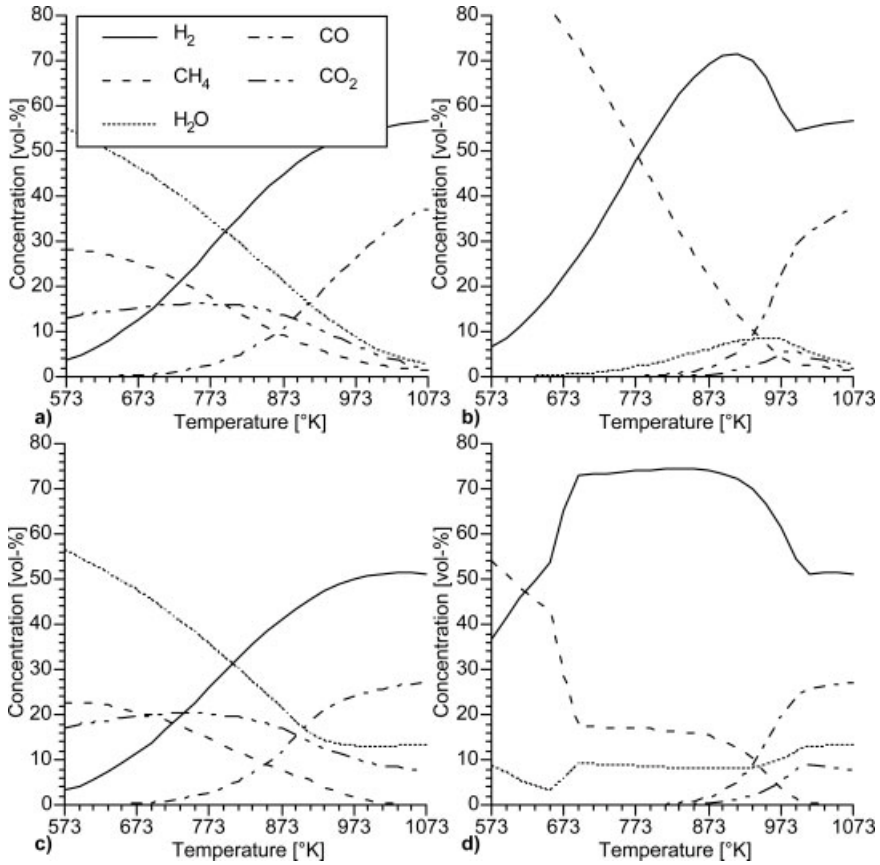


**Figure 2. Predicted product gas composition for biomass decomposition: (a) without steam or CaO; (b) without steam and with CaO (C-to-Ca ratio is 1:1 on a molar basis); (c) with steam (C-to-$H_2O$ ratio is 1:1 on a molar basis), without CaO; (d) with steam (C-to-$H_2O$ ratio is 1:1 on a molar basis) and CaO (C-to-Ca ratio 1:1 on a molar basis).**

Data presented in (c) and (d) is Reproduced from Ref 18, with permission from Elsevier Science.

A commercial modeling package, Factsage 5.4.1 (EQULIB module), was used. Cellulose was chosen as a model biomass fuel (Table 2). The model predictions demonstrate the influence of operating conditions including temperature, steam-to-carbon feed ratio, and the presence of CaO on the equilibrium distribution of product species.

Figure 2 shows the gaseous products of biomass conversion with and without additional $H_2O$ (g) and CaO (s) present. The reaction system was investigated at atmospheric pressure over a temperature range from 573 to 1073 K. The concentrations (vol %) of $H_2$, $CH_4$, $H_2O$, CO, and $CO_2$ are displayed as a function of temperature. Although a more comprehensive list of gaseous species was included in the equilibrium study (i.e. higher hydrocarbons, oxy-, and nitro-compounds), they were not predicted to be present at equilibrium under the conditions considered. Clearly, the presence of a broader range of products of biomass conversion (shown in "Results and Discussion") suggests either that there is insufficient time for these products to reach equilibrium composition or that the formation mechanism deviates from thermodynamic equilibrium. In either case, discrepancies between equilibrium predictions and experimental results demonstrate the importance of nonequilibrium phenomena, e.g. (i) heating rate, (ii) the evolved gas residence time, and (iii) the likely catalytic role of CaO and/or $CaCO_3$.

Figure 2a shows the predicted products of biomass conversion without steam and CaO. An increase in the $H_2$ concentration is observed corresponding with an increase in the reaction temperature from 573 to 1073 K. A maximum $H_2$ concentration of 56.5 vol % is observed at 1073 K. Similarly, an increasing trend is observed for CO. These predictions highlight the importance of the endothermic reactions, i.e. Eqs. 2–4, 7, and 8, for $H_2$ and CO production. By contrast, a decreasing trend is observed for $CH_4$ and $H_2O$ and a maximum $CO_2$ concentration of 16.2 vol % is predicted at 773 K.

The predicted influence of CaO on the pyrolysis of biomass is shown in Figure 2b. A dramatic increase in the $H_2$ concentration is observed when CaO is present. In this case, an increase in $H_2$ concentration corresponds to an increase in temperature to a maximum of 71.6 vol % at 913 K. Effective capture of $CO_2$ by CaO is observed for the temperature range from 573 to 913 K, with a $CO_2$ concentration of less than 1.3 vol %. Furthermore, the reduction in the CO concentration in this temperature range suggests the importance of the water–gas shift reaction, according to Eq. 1, for influencing the $H_2$ output. The $CH_4$ concentration in the low temperature

**Table 2. Proximate and Ultimate Analysis of Methyl Cellulose**

| Proximate Analysis | | Ultimate Analysis | |
|---|---|---|---|
| | % wt (Dry Basis) | Element | % wt (Dry Basis) |
| Ash yield | 1.2 | C | 49.3 |
| Volatile matter | 87.6 | H | 7.2 |
| Fixed carbon | 11.2 | O | 42.1 |
| Moisture | 5.7 (%) | N | <0.01 |
| | | S | 0.21 |

range (573–773 K) is consistent with the exothermic methanation process, according to Eq. 12. The decline in the $H_2$ concentration and the increase in the $CO_2$ concentration at temperatures above 913 K are consistent with the decomposition of $CaCO_3$ according to the endothermic calcination reaction, favored at high temperatures.

The influence of steam on the biomass conversion products is shown in Figure 2c (without CaO present). A maximum $H_2$ concentration of 51.5 vol % is predicted at 1033 K. In addition, a reduction in the $CH_4$ concentration and an increase in the $H_2O$, CO, and $CO_2$ concentrations are observed for the range of temperatures investigated (compared to those presented in Figure 2a). Generally, these differences in the product gas distribution may be explained on the basis of an increase in the char conversion, which is at equilibrium with the gaseous product. Obviously, enhanced char conversion results in an increase in the total product gas yield.[18] These general trends may be inferred from the equations shown in Table 1. Obviously, maximizing both the extent of biomass conversion and the $H_2$ concentration is desirable.

The effect of CaO on the equilibrium product gas distribution for biomass conversion with steam is displayed in Figure 2d. In this case, a broad operating window with respect to temperature, from 733 to 873 K, is predicted for maximizing the concentration of $H_2$ and for minimizing the concentrations of CO and $CO_2$. Within this temperature range a maximum $H_2$ concentration of 74.5 vol % is predicted. In addition, a further increase in the $H_2$ concentration to 81.4 % vol (dry) is calculated assuming that the steam (predicted at 8–9 vol %) is condensed. The CO and $CO_2$ concentrations are maintained below 1.6 vol % and 0.5 vol %, respectively. These very low carbon oxide concentrations are indicative of the effective $CO_2$ capture with CaO according to Eq. 13 and the importance of the water–gas shift reaction, Eq. 1.

Previous experimental studies confirm thermodynamic equilibrium model predictions and demonstrate the potential for enhanced $H_2$ synthesis in biomass gasifiers combined with $CO_2$ removal.[16,17,19,20] Hanaoka et al.[20] investigated steam gasification of "Japanese oak" with $Ca(OH)_2$ using a pressurized batch reactor (i.d. 50 $cm^3$). They reported a maximum $H_2$ concentration of 84.8 % vol (dry) at 873 K and $1.3 \times 10^6$ bar.

Pfeifer et al.[16,17] reported a maximum $H_2$ concentration of 75 vol % (dry) at 973 K using an atmospheric pressure, dual fluidized bed gasifier (pilot-plant, 100 kwth) with CaO and a Ni-olivine catalyst (10% wt) as the bed material.

In light of the thermodynamic model predictions and promising experimental data from the literature, the potential merit of the combined gasification/$CO_2$ removal process is apparent. However, the fundamental mechanism is not well understood. In this work, we have carried out a simultaneous thermogravimetric-mass spectrometric (TG-MS) study in order to elucidate the important reaction pathways and to obtain data relevant to the design and scale-up of novel biomass gasifiers with in-situ $CO_2$ removal using CaO.

### *Cellulose pyrolysis*

An understanding of the fundamental chemical mechanism of biomass pyrolysis is essential for the design and optimization of novel biomass gasifiers. Because of the fact that dry biomass fuels are typically composed of approximately 50% wt cellulose, the mechanism of cellulose pyrolysis and the distribution of cellulose pyrolysis products have been extensively studied.[21–31]

A large range of cellulose pyrolysis products have been identified, including $H_2$, $H_2O$, CO, $CO_2$, levoglucosan, char, aldehydes, ketones, and organic acids.[21–31] The extent of this product list highlights the complexity of the decomposition process.

A generally accepted reaction mechanism involves two competing reaction pathways.[21,22,25,32] (i) One reaction pathway involves a depolymerization or "unzipping" process that leads primarily to the formation of levoglucosan. Levoglucosan may decompose further via secondary reactions to yield tars, gases and char. (ii) The second pathway involves the direct fragmentation of cellulose (i.e. "ring scission") leading to the formation of glycoaldehyde as a primary product. Further decomposition results in gas and char production. A comprehensive discussion of the chemistry underpinning these competing reaction pathways is available in the literature.[21,22,25,32]

Previous investigators have examined a range of factors affecting the relative importance of these competing reaction pathways. Of particular relevance to this work are: (i) the influence of inorganic ions, (ii) the nature of evolved gas/decomposing solid interactions, and (iii) the influence of additional water vapor.

The dramatic influence of inorganic ions, which include trace mineral matter that is naturally present in biomass, as well as additives, has been widely reported.[21,26,28,32] Piskorz et al.[32] examined the distribution of decomposition products following a pretreatment with sulfuric acid for the removal of mineral matter (in this case 1700 ppm $K^+$, 50 ppm $Na^+$, and 1200 ppm $Ca^{2+}$). They concluded that the presence of trace amounts of alkali and earth alkali cations inhibits the "unzipping" process leading to the formation of levoglucosan. Similarly, Richards and Zheng[26] reported a decrease in the amount of tar and levoglucosan and an enhanced char yield when $K^+$, $Li^+$, and $Ca^{2+}$ were present during vacuum pyrolysis. Varhegyi et al.[28] systematically investigated the influence of a range of additives (1 mol % wt) including $MgCl_2$, NaCl, $FeSO_4$, and ZnCl on the pyrolysis of pure cellulose, using a TG-MS. They reported a host of effects highlighting the dramatic and complex influence of mineral matter on cellulose decomposition. Because of the small amount of catalyst used (1 mol % wt), and thus the relatively limited contact between the catalyst and the cellulose, they contend that the "long range catalytic effects" of mineral matter are

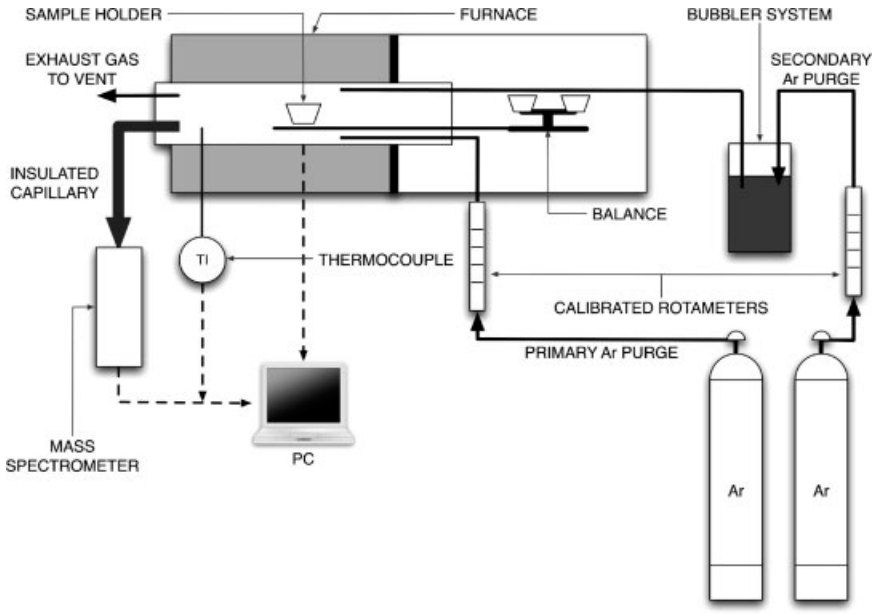


**Figure 3. Modified thermogravimetric analyzer/mass spectrometer (TG-MS) for the decomposition of biomass fuels and the simultaneous analysis of evolved product gas species.**

most significant in influencing the final product distribution, which is consistent with the literature.

Several investigators have studied the nature of gas–solid interactions effecting char formation.[21,24,30] Mok et al.[24] conducted pyrolysis experiments using sealed reaction vessels that inhibit the escape of evolved gases. The increase in the partial pressure of water vapor, which is a major product of cellulose pyrolysis, was reported to correspond with a significant increase in char formation (up to 40% wt) as well as a shift in the $T_{peak}$ to a lower temperature.[24] On the basis of these observations, it was concluded that water vapor catalyses the gas–solid interactions leading to char formation.[21,24,30]

These previous studies clearly demonstrate the potential for manipulating the major mechanistic pathways underpinning cellulose decomposition.

## Experimental

### *TG-MS*

Experiments were carried out using a modified thermogravimetric analyzer (TA-SDTQ6000) coupled with a mass spectrometer (Pfeiffer Vacuum/ThermoStar-GSD301/qudrupole mass analyzer) (TG-MS). A schematic of the experimental apparatus is given in Figure 3.

The TG-MS measures the pyrolytic weight loss using a thermobalance (sensitive to 0.01 mg). Evolved pyrolysis gases are flushed from the vicinity of the decomposing solid with an Ar purge (500 mL/min) and a sample of these evolved gases is delivered to the mass spectrometer via a heated capillary. Mass spectra of the evolved gases are recorded as a function of temperature using the mass spectrometer. The main advantage of the TG-MS technique for this study is the rapid data acquisition whereby the evolved species can be sampled in real time corresponding to pyrolytic decomposition of the biomass. Thus, we are able to record the changes in the mass spectra affected by changing the pyrolysis conditions. A comparison of the rate of weight loss with the mass spectra was used to elucidate the different mechanistic pathways involved in the decomposition process.

For pyrolysis experiments conducted in the presence of water vapor, a bubbler system was used. Ar was bubbled through degassed water heated to 333 K. The amount of water in the wet gas stream was determined by calculating the mass fraction of $H_2O$, assuming the Ar-$H_2O$ vapor mixture was saturated. At 333 K and atmospheric pressure the mass fraction of $H_2O$ in Ar is approximately 0.1 (wt/wt). To avoid condensation prior to delivery of the wet gas to the furnace, the wet gas line was heated to 353 K using heating tape. The amount of water vapor was adjusted by controlling the Ar flow rate to the bubbler system while the total Ar purge flow rate was adjusted to maintain a constant total purge flow rate. The wet gas was introduced to the furnace when the furnace temperature exceeded 383 K. Observance of a steady ion current signal for $m/z = 18$ indicated that a constant rate of delivery was achievable using the bubbler system.

Selected experiments were conducted using a capped reaction vessel. These experiments were performed to examine the influence of the evolved gas residence time and the corresponding effects of enhanced sorbent utilization and evolved gas/decomposing solid interactions. For these experiments, an alumina disc was placed on top of the sample holder and the evolved gases could only escape when the pressure inside the reaction vessel was sufficient to displace the lid. We were unable to quantify the change in residence time because of the influence of secondary interactions.

The coupled TG-MS system has limitations. (i) Some fraction of the tar produced during the decomposition is not detected by the mass spectrometer because heavy species

may condense on the capillary or furnace walls. For example, Varhegyi et al.,[28] using a similar method (capillary heated to 453 K), estimated the nondetected tar fraction to be as high as 50–70% wt for pure cellulose pyrolysis (heating rate 10°K/min). Similarly, Fushimi et al.[33,34] estimated the tar fraction for cellulose pyrolysis to be 81% wt (heating rate of 1°K/min). These estimates are consistent with this work, in fact we did not observe mass spectra data for species with a mass to charge ratio ($m/z$) greater than 110. To minimize the condensation of volatiles the capillary is housed in an insulated sheath which was heated to 473 K. (ii) Obtaining a representative sample of the volatiles using a capillary can be problematic.[28,29] In this work, the insertion and positioning of the capillary in the furnace was consistent for all experimental runs. The vacuum pressure was monitored for fluctuations, which may indicate a blockage in the capillary or orifice.

### *Mass spectra, identification of probable molecules, and quantification of permanent gas yield*

The analysis of gas molecules by mass spectrometry principally involves bombarding the molecules with a beam of electrons. This process results in the production of a positive molecular ion, which are distinguished based on their mass to charge ratio ($m/z$). Typically, the electron beam energy (in this case 70 eV) is greater than the amount of energy required to achieve ionization and the excess energy results in severe fragmentation of the primary molecular ion.[35] This process results in a mass spectrum, representing a range of positively charged fragment ions, which is characteristic of a probable parent molecule.[35] For example, $CO_2$ is the probable parent molecule corresponding $m/z = 44$ ($CO_2^+$). Because of the fragmentation process, a number of minor signals are detected, including $m/z = 6$, 12, 28, 29, and 45.

A preliminary broad scan was conducted for the decomposition of pure cellulose, which is involved in the observance of ion current signals from 1 to 200 m/z. On the basis of the preliminary scan, a list of key molecular ions was compiled by rejecting signals when the maximum intensity was close to the noise level, as well as conducting a thorough cross check with the relevant literature.[22,28,29] The complete list of molecular ions that were detected (and the probable parent molecules) is given in Table 3. It is apparent that the method is biased towards low molecule weight species, which is suitable for the objective of maximizing the $H_2$ output.

Two methods were employed to confirm the reliability of the TG-MS technique and derive quantitative data for the permanent gases. (i) The first method involved experiments using calcium oxalate monohydrate. Results confirming the reliability of the TG-MS methodology are presented in "Reliability of TG-MS method." (ii) A synthetic product gas mixture composed of 10 vol % $CH_4$, 20 vol % CO, 35 vol % $H_2$, and 35 vol % $CO_2$ was introduced to the TG-MS at various flow rates (0–60 $cm^3$/min) in order to determine the relationship between ion current intensity and permanent gas yield. These experiments were carried out after each pyrolysis experiment to establish the reliability of the MS for detecting changes in the permanent gas yield and to monitor fluctuations in the ion current intensity affecting the reproducibility of the results (likely associated with contamination of the instrument and normal degradation of the of the ion source). The total vacuum pressure was monitored for variations, which may indicate a blockage in the capillary or orifice, and thus influence the delivery of the evolved gas to the vacuum chamber.

**Table 3. Key Molecular Ions/Ion Fragments and Probable Parent Molecules**

| $m/z$ | Key Molecular Ions/ Ion Fragments | Probable Parent Molecule |
|---|---|---|
| 2 | $H_2^+$ | $H_2$ |
| 12 | $C^+$ | CO, $CO_2$, $C_xH_y$ |
| 15 | $CH_3^+$ | $CH_4$, $C_xH_y$ |
| 16 | $O^+$, $CH_4^+$ | $CH_4$, $H_2O$ |
| 18 | $H_2O^+$ | $H_2O$ |
| 26 | $C_2H_2^+$ | $C_xH_y$ |
| 27 | $C_2H_3^+$ | $C_xH_y$ |
| 28 | $C_2H_4^+$, $CO^+$ | CO, $CO_2$, $C_2H_4$ |
| 29 | $C_2H_5^+$ | Aldehydes |
| 30 | $C_2H_6^+$ | Formaldehyde |
| 31 | $C_2H_2OH^+$ | $C_2H_3OH$ (methyl alcohol, glycoaldehyde) |
| 32 | $CH_4O^+$ | Methanol |
| 43 | $C_3H_7^+$, $C_2H_3O^+$ | $C_xH_y$,$C_2H_5OH$ |
| 44 | $C_3H_8^+$, $CO_2^+$, $C_2H_4OH^+$ | $CO_2$ |
| 45 | $C_2H_5O^+$ | $C_2H_5OH$ |
| 58 | $(CH_3)_2CO^+$ | $C_3H_6O$ (acetone) |
| 68 | $C_4H_4O^+$ | $C_4H_4O$ (furan) |
| 74 | $C_3H_6O_2^+$ | Acetol |
| 84 | $C_4H_4O_2^+$ | 2(5H)-furanone |
| 96 | $C_5H_4O_2^+$ | Furfural |
| 110 | $C_6H_6O_2$ | $C_6H_6O_2$ (5-methyl furfural, dihydroxybenzenes) |

### *Test samples and sample preparation*

Cellulose (methyl cellulose LR/Chem Supply) was selected as a model biomass species. It was mentioned in "Previous Experimental Studies" that cellulose pyrolysis has been studied extensively. Importantly, the decomposition of pure cellulose closely reflects the decomposition behavior of the cellulose component of biomass. Equally, the decomposition of biomass behaves as the sum of its constituents and cellulose is the major component, usually of the order of 50% wt.[21,22] Furthermore, the main products of the gasification of biomass can be correlated to the cellulose content.[11,19]

Approximately 5 mg of cellulose was loaded into the sample holder for all experiments. Pyrolytic decomposition was conducted at three different heating rates: 5°K/min, 40°K/min, and 100°K/min. The selection of the sample size, the distribution of the sample in the sample pan, and the rate of heating have a significant influence on the reaction kinetics, due to heat and mass transfer effects.[23] Small samples ($\leq$5 mg) are advisable for achieving reproducible kinetic data.[21,23] However for TG-MS, a lower limit on the sample size of 5 mg was imposed due to the sensitivity of the mass spectrometer.

CaO was prepared by calcining $CaCO_3$ (Sigma Aldrich/ sieved to $<45$ $\mu$m) under $N_2$ at 973 K, for 2 h. Calcination conditions were selected to lessen the effect of sintering of CaO and thus produce a highly reactive $CO_2$ sorbent.[36] The cellulose and CaO were mixed in situ in order to minimize

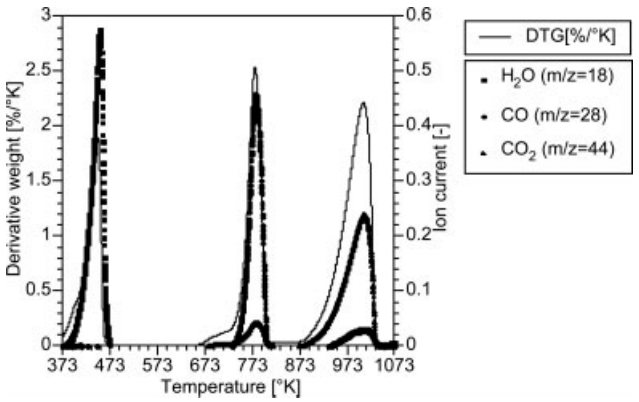


**Figure 4. Derivative weight loss curve and mass spectra for the decomposition of calcium oxalate monohydrate.**

the exposure of the fresh sorbent to atmospheric water vapor and $CO_2$. CaO was loaded at a ratio of Ca:C of 1 and 0.5 for select experiments.

## Results and Discussion

### *Reliability of the TG-MS method*

Calcium oxalate monohydrate is commonly used to demonstrate TGA performance because the decomposition to CaO gives three distinct weight loss events associated with the evolution of $H_2O$, CO, and $CO_2$. This common decomposition experiment can also be used to demonstrate the performance of the TG-MS technique.[28,29] Figure 4 shows the derivative weight loss curve and mass spectra for the decomposition of calcium oxalate monohydrate. The decomposition of calcium oxalate monohydrate was conducted at a moderate heating rate (20°K/min) with a high Ar purge (500 mL/min), i.e. equivalent to the conditions used for cellulose decomposition. The first decomposition peak is associated with the evolution of $H_2O$ ($m/z$ = 18). The second decomposition is associated with the evolution of CO ($m/z$ = 28). A minor ion current signal for $CO_2$ ($m/z$ = 44) corresponding the second decomposition step shows the disproportionation of CO to $CO_2$ and C. Further evidence of this phenomenon was the observance of a carbon residue which coated the CaO at the conclusion of the decomposition experiment. The third and final decomposition peak is associated with the evolution of $CO_2$ ($m/z$ = 44). In the case, the additional ion current signal for $m/z$ = 28 may be associated with the fragment ion $CO^+$. Mass spectra for additional key ion fragments of $H_2O$, CO, and $CO_2$ including $m/z$ = 6, 12, 16, 17, and 29 are not displayed for clarity of presentation.

Importantly, the good fit of the derivative weight curve and the mass spectra clearly demonstrates the reliability of the method adopted in this work.

### *Reproducibility of thermogravimetric (and mass spectrometric) data*

Three pure cellulose pyrolysis experiments were conducted at a moderate heating rate (40°K/min) in order to demonstrate the reproducibility of the TG and MS data.

The derivative weight curves for the three experimental runs are displayed in Figure 5. The good agreement between the three experimental trials clearly demonstrates the reproducibility of the pyrolytic decomposition of pure cellulose. The single and uniform decomposition peak is consistent with decomposition profiles in the literature for pure cellulose, in the absence of mineral impurities and catalysts, and when heat and mass transfer phenomena is limited.[21,23] Select thermogravimetric data is tabulated in Table 4. In all cases the decomposition commences around 543 K. $T_{peak}$, defined as the temperature corresponding the maximum rate of decomposition, is 656.5 K, 656 K, and 655.6 K for runs 1, 2, and 3, respectively. Some variation is observed in the final char content. The final char content is defined as the amount of char at 773 K and is represented as a percentage of the initial dry sample mass. Final char content was 14.3 wt %, 14.7 wt %, and 11.2% for runs 1, 2, and 3, respectively. Moreover, the variation highlights the complexity of the decomposition mechanism. In this case, with pure cellulose, experimental variability such as the distribution of the sample in the sample pan or a nonhomogenous nature of the sample may influence the rate of escape of the evolved volatiles and thus the relative dominance of different decomposition pathways. Mechanisms of char formation are discussed in "Char formation."

The corresponding mass spectrometric data for these repeat trials is presented in Table 4. Ion current data is expressed in terms of relative ion current intensity and was determined by integration of the mass spectra and presented as a fraction of the total ion current signal area. This approach was adopted to minimize variations in the baseline intensity and to minimize systematic error associated with fluctuations in the ion current throughout the course of experiments. The reasonable reproducibility of the relative ion current data demonstrates the reliability of the results. Minor variations in this data provide further evidence of the complexity of the decomposition mechanism.

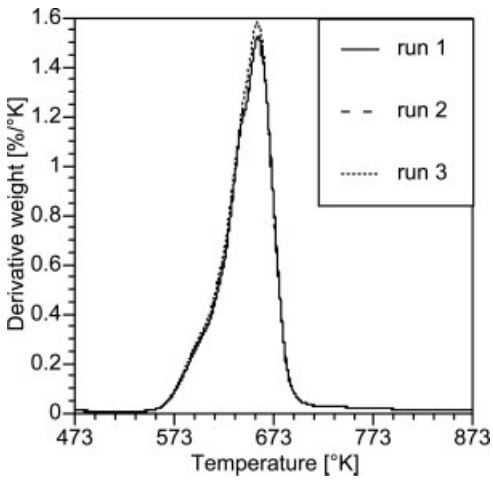


**Figure 5. Derivative weight loss curves for three pure cellulose decomposition experiments all conducted at a heating rate of 40°K/min with an Ar purge (500 mL/min).**

**Table 4. Relative Ion Current Intensities for Evolved Species During Cellulose Pyrolysis***

| *m/z* | Probable Parent Molecule | Cellulose** (40°K/min) | Cellulose (100°K/min) | Cellulose (40°K/min; w/lid) | Cellulose (40°K/min; wg = 50 mL/min) | Cellulose and CaO (Ca:C = 1; 40°K/min) | Cellulose and CaO (Ca:C = 1; 40°K/min; w/lid) | Cellulose and CaO (Ca:C = 0.5; 40°K/min; w/lid) | Cellulose and CaO (Ca:C = 1; 40°K/min; wg = 50 mL/min) | Cellulose and CaO (Ca:C = 0.5; 40°K/min; wg = 50 mL/min) |
|---|---|---|---|---|---|---|---|---|---|---|
| 2 | $H_2$ | nd† | 0.000 | 0.000 | 0.000 | 0.003 | 0.005 | 0.003 | 0.003 | 0.002 |
| | | nd | | | | | | | | |
| | | nd | | | | | | | | |
| 15 | $CH_4$ | 0.110 | 0.106 | 0.104 | 0.104 | 0.064 | 0.061 | 0.079 | 0.063 | 0.070 |
| | | 0.101 | | | | | | | | |
| | | 0.086 | | | | | | | | |
| 18 | $H_2O$ | 0.199 | 0.173 | 0.222 | 0.205 | 0.559 | 0.513 | 0.417 | 0.533 | 0.493 |
| | | 0.219 | | | | | | | | |
| | | 0.222 | | | | | | | | |
| 26 | $C_xH_y$ | 0.007 | 0.011 | 0.005 | 0.005 | 0.003 | 0.002 | 0.004 | 0.003 | 0.003 |
| | | 0.006 | | | | | | | | |
| | | 0.009 | | | | | | | | |
| 27 | $C_xH_y$ | 0.016 | 0.021 | 0.013 | 0.013 | 0.007 | 0.007 | 0.010 | 0.007 | 0.008 |
| | | 0.012 | | | | | | | | |
| | | 0.020 | | | | | | | | |
| 28 | CO | 0.101 | 0.155 | 0.085 | 0.096 | 0.047 | 0.055 | 0.064 | 0.046 | 0.058 |
| | | 0.103 | | | | | | | | |
| | | 0.118 | | | | | | | | |
| 29 | Aldehydes | 0.129 | 0.118 | 0.122 | 0.128 | 0.080 | 0.074 | 0.100 | 0.079 | 0.085 |
| | | 0.123 | | | | | | | | |
| | | 0.126 | | | | | | | | |
| 30 | Formaldehyde | 0.021 | 0.028 | 0.019 | 0.021 | 0.011 | 0.011 | 0.017 | 0.011 | 0.012 |
| | | 0.022 | | | | | | | | |
| | | 0.029 | | | | | | | | |
| 31 | Glycoaldehyde | 0.119 | 0.103 | 0.124 | 0.125 | 0.104 | 0.108 | 0.107 | 0.098 | 0.097 |
| | | 0.122 | | | | | | | | |
| | | 0.117 | | | | | | | | |
| 32 | $CH_4O$ | 0.067 | 0.059 | 0.069 | 0.072 | 0.063 | 0.067 | 0.063 | 0.057 | 0.057 |
| | | 0.072 | | | | | | | | |
| | | 0.072 | | | | | | | | |
| 43 | Acet/pyruv-aldehyde | 0.020 | 0.019 | 0.019 | 0.020 | 0.007 | 0.012 | 0.017 | 0.008 | 0.008 |
| | | 0.017 | | | | | | | | |
| | | 0.014 | | | | | | | | |
| 44 | $CO_2$ | 0.069 | 0.064 | 0.080 | 0.076 | 0.009 | 0.008 | 0.015 | 0.008 | 0.018 |
| | | 0.073 | | | | | | | | |
| | | 0.076 | | | | | | | | |
| 45 | $C_2H_5OH$ | 0.074 | 0.052 | 0.071 | 0.076 | 0.003 | 0.031 | 0.052 | 0.041 | 0.046 |
| | | 0.067 | | | | | | | | |
| | | 0.047 | | | | | | | | |
| Final char content‡ | | 14.3 | 8.7 | 9.5 | 13.6 | 16.8 | 6.4 | 15.6 | 0.7 | 20.6 |
| | | 14.7 | | | | | | | | |
| | | 11.4 | | | | | | | | |
| $T_{peak}$ (DTG) | | 656.5 | 674.2 | 666.8 | 655.3 | 648.3 | 655.4 | 655.8 | 649.6 | 650.8 |
| | | 656.0 | | | | | | | | |
| | | 654.6 | | | | | | | | |

*The ion current intensities were determined by integration of the mass spectrometric peak for evolved species corresponding the primary decomposition. Other information could be reported, e.g. peak intensity, however, the area under the peak was considered most accurate because of variable baseline intensity and high noise levels. The selection of both the point of initiation and the end point defining the mass spectrometric peak has a significant influence on the determination of area under the curve. In some cases the peaks included a slow tailing section, which may be attributed to a slow charring process.[28] The merging of primary and secondary peaks was also observed. For consistency, we did not include the additional area associated with a peak tail or the additional area associated with secondary decomposition peak if this area was beyond 773 K. The relative ion current intensity data was determined by summing the total area data for the complete range of ion current signals and representing each signal as fraction of this total area. This approach was taken in order to minimize systematic error associated with fluctuations in the ion current intensity throughout the course of the experimental program.

**To determine the reproducibility of the pyrolysis experiments we ran two repeat tests for pure cellulose decomposition at a heating rate of 40°K/min.

†No data (nd) was recorded when the magnitude of the noise is of the same order as the signal maximum. This does not imply that the species was not present, rather that we are unable to detect it.

‡Final char content is reported at 773 K. At a temperature of 773 K, pyrolytic decomposition was complete for all experimental conditions investigated. For experiments with CaO, the char content at 773 K was determined by subtracting the weight of the reacted sorbent. We estimated the extent of sorbent utilization based on thermogravimetric data corresponding the sorbent decomposition, according to Eq. 14.

### *Influence of heating rate on pyrolysis kinetics*

Experiments were conducted at three heating rates, that is 5, 40, and 100°K/min. The effect of heating rate on the cellulose pyrolysis kinetics, represented in terms of the rate of weight loss as a function of temperature, is displayed in Figure 6. A shift in the decomposition peak, indicating a thermal lag corresponding to an increase in the heating rate was observed. $T_{peak}$ is 613.1, 656, and 674.2 K for heating at 5, 40, and 100°K/min, respectively. This increase in $T_{peak}$ at higher heating rates is consistent with the literature[23] and may be attributed to heat and mass transfer effects. A reduction in the sample mass at higher heating rates is expected to offset the thermal lag to some extent, however in this case, a constant sample mass of approximately 5 mg was used due to the sensitivity of the mass spectrometer. Interestingly, the heating rate does not appear to influence the general decomposition profile and a single and uniform peak is observed for all heating rates. This suggests that the decomposition mechanism is not fundamentally affected by the heating rate under the range of conditions investigated. Moreover, it may be concluded that the experimental procedure used minimizes the influence of heat and mass transfer, which might affect the decomposition pathway at different heating rates.

The relative ion current intensity data does show minor variations in the detectable gas products because of heating rate (Table 4). For example, the relative ion current intensity data for cellulose pyrolysis at a heating rate of 5°K/min compared to 40°K/min suggests a minor increase in the relative amount of aldehydes ($m/z$ = 29, 30, and 31) and a minor decrease in the relative amounts of CO, $H_2O$, and higher hydrocarbons. In contrast, an increase in the CO and higher hydrocarbon concentration was observed for a heating rate of 100°K/min. These minor variations can be accounted for in terms of the extent of the secondary interactions between the evolved gases and the decomposing solid. Specifically, the extent of interaction is expected to be greater at a faster heating rate due to heat transfer limitations resulting in an inconsistent rate of decomposition throughout the sample. Although, this effect is minimized by using a small cellulose sample, the significance of secondary gas–solid interactions is well known and discussed in "Char Formation."[24,30]

### *Influence of CaO on cellulose pyrolysis*

To investigate the influence of CaO on the decomposition of cellulose, experiments were conducted, with and without CaO present.

The pyrolysis kinetics of cellulose is dramatically influenced by the presence of CaO. $T_{peak}$ for cellulose decomposition with and without CaO are presented in Table 4. At heating rates of both 5 and 40°K/min a decrease in $T_{peak}$ of 6.3°K and 7.7°K was observed, respectively. The observed shift in $T_{peak}$ can be attributed to a number of factors that are expected to affect the rate of weight change: (i) primarily, the concurrent $CO_2$ capture reaction (as well as sorbent hydration) will result in an increase in the sample weight; (ii) these exothermic gas–solid absorption reactions generate additional heat which potentially contributes to a self-heating effect; (iii) furthermore, particle swelling associated with the carbonation and hydration process (due to the higher molar volume of $CaCO_3$ and $Ca(OH)_2$) may influence the rate at which the evolved gases escape from the decomposing solid; (iv) heat transfer effects are expected when CaO is loaded (Ca:C = 1 molar basis) associated with the significantly larger sample mass; (v) finally, CaO may directly catalyze the decomposition of cellulose. We are unable to deduce which is the dominant mechanism based solely on a shift in $T_{peak}$. However, given the shift in $T_{peak}$ is of a comparable magnitude for both heating rates, the heat transfer effects may be of limited importance under the conditions investigated.

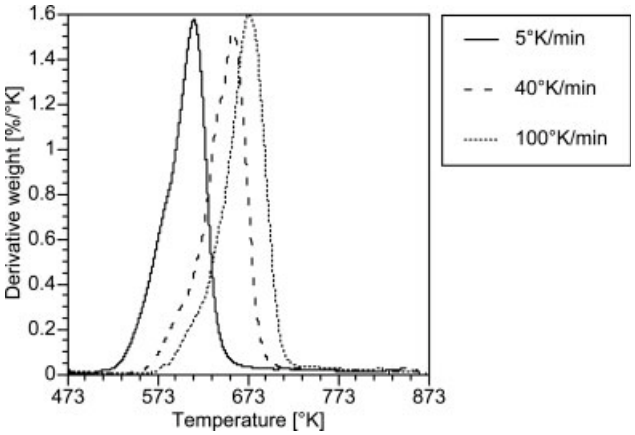


**Figure 6. Effect of heating rate on cellulose pyrolysis kinetics (without CaO and without additional $H_2O$ vapor).**

To gain an insight into the importance of the different decomposition mechanisms we compare the mass spectra corresponding with the decomposition of cellulose, with and without, CaO present. Figures 7a–d shows the mass spectra for the evolved species as a function of temperature corresponding to the decomposition of cellulose, with and without CaO. Figure 7a shows cellulose decomposition without CaO at a moderate heating rate of 40°K/min. The rate of cellulose decomposition (represented in terms of the derivative weight loss [%/°K]) is shown in bold and the mass spectra for the evolved gas species are plotted as a function of temperature. The permanent gases are presented in Figure 7a, i.e. $H_2$ ($m/z$ = 2), $CH_4$ ($m/z$ = 15), $H_2O$ ($m/z$ = 18), CO ($m/z$ = 28), and $CO_2$ ($m/z$ = 44). For clarity of presentation, additional evolved gas species, including higher hydrocarbons $C_2H_y$ ($m/z$ = 26 and 27 assigned to $C_2H_2^+$ and $C_2H_3^+$, respectively) and aldehydes ($m/z$ = 29, 30, 31, 43) are presented in Figure 7b. The scale is deliberately omitted on the vertical axis because the ion current data was scaled to a zero baseline and the magnitude of the derivative weight loss curve is not directly comparable between experiments with and without CaO. The range of species displayed in Figure 7 does not imply that no other species were identified. Only major species and those representing important classes of species are shown for clarity.

The close fit between the derivative weight loss curve and the evolved gas species, including both the permanent gases (Figure 7a) as well as the higher hydrocarbons and aldehydes (Figure 7b) confirms that the decomposition of pure cellulose is dominated by a single step reaction mechanism.[21,28]

For comparison, the decomposition of cellulose when CaO is present (Ca:C = 1 molar basis) is displayed in Figures 7c,d.

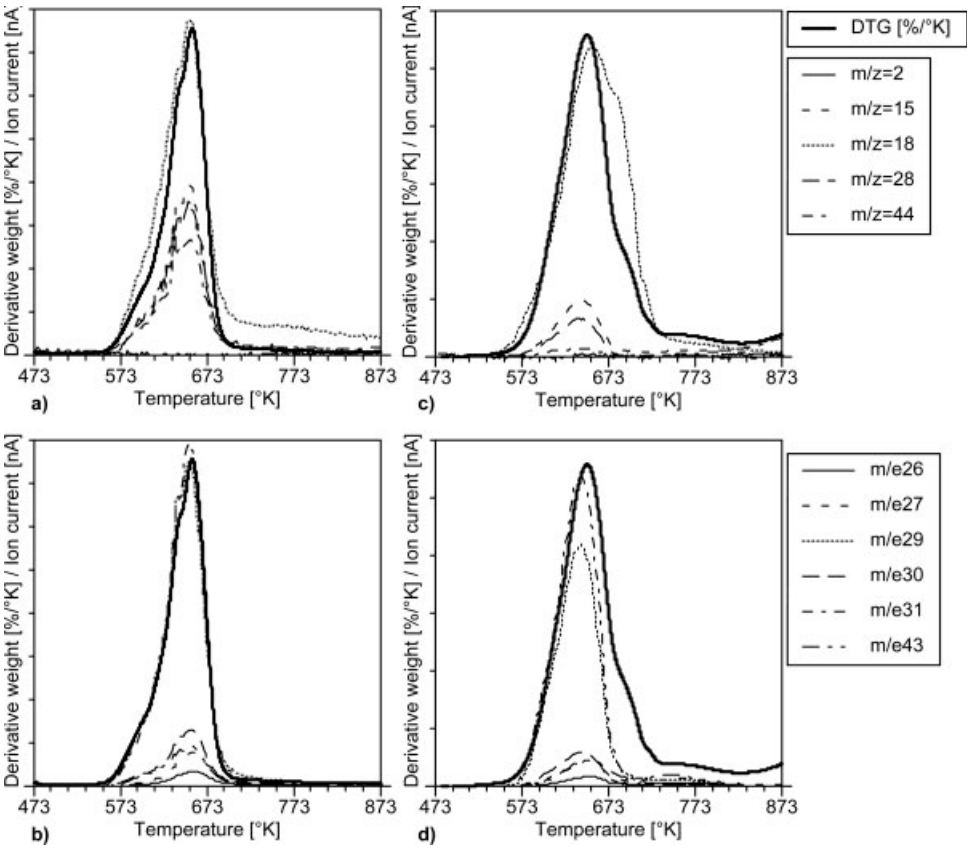


**Figure 7. Mass spectra for the evolved species for the decomposition of cellulose, with and without CaO.**

(a) Cellulose decomposition without CaO (heating rate 40°K/min). The bold line represents the derivative weight curve (DTG, %/°K) and the dashed lines correspond with the mass spectra as a function of temperature assigned to the permanent gases, i.e. $H_2$ ($m/z$ = 2), $CH_4$ ($m/z$ = 15), $H_2O$ ($m/z$ = 18), CO ($m/z$ = 28), and $CO_2$ ($m/z$ = 44). For clarity of presentation, additional evolved gas species, including higher hydrocarbons $C_2H_y$ ($m/z$ = 26 and 27 assigned to $C_2H_2^+$ and $C_2H_3^+$, respectively) and aldehydes ($m/z$ = 29, 30, 31, 43) are presented in (b). (c) Cellulose decomposition in the presence of CaO (heating rate 40°K/min; Ca:C = 1 molar basis). Again, for clarity of presentation, additional evolved gas species are shown separately in (d). No scale is given for the vertical axis because the ion current data was scaled to a zero baseline and the magnitude of the derivative weight loss curve is not directly comparable between experiments, with and without CaO.

The derivative weight loss curve when CaO is present is significantly broader compared to decomposition without CaO. The additional breadth reflects an earlier initial weight loss (by approximately 20°K) and a secondary, slower decomposition step commencing at approximately 673 K. It is apparent that the weight loss associated with the secondary decomposition step is solely associated with the evolution of $H_2O$ (i.e. $m/z$ = 18) and not accompanied by the production of other key species. In light of this, it is likely that the secondary decomposition step corresponds with the decomposition of $Ca(OH)_2$ according to Eq. 15, rather than due to dehydration or secondary cracking reactions. The observance of additional $H_2O$ via the proposed mechanism is consistent with thermodynamic equilibrium predictions and implicates the exothermic sorbent hydration as an important mechanism during cellulose decomposition in the presence of CaO.

$$Ca(OH)_2 \rightarrow CaO + H_2O \quad \Delta H^0_{873.15} = -97.8\,\mathrm{kJ/mol} \quad (15)$$

Noteworthy displacement in the temperature between the maximum ion current intensities for the evolved species and $T_{peak}$ (DTG) was observed when CaO is present. The temperature corresponding the ion current peak intensity for $H_2$ (5.2°K), $CH_4$ (7.2°K), $CO_2$ (13.0°K), and aldehydes ($m/z$ = 29, 31, 6.7°K, 6.6°K, respectively) are observed to precede $T_{peak}$. In contrast the $H_2O$ peak is recorded at a temperature 6°K higher than $T_{peak}$. This displacement is consistent with the sorbent hydration mechanism. The close alignment of the permanent gases and the aldehydes likely indicates that these gases are evolved via the same mechanistic pathway, consistent with direct fragmentation. The most significant displacement is observed for $CO_2$, which is due to the $CO_2$ capture mechanism. Given the low estimated extent of sorbent utilization (6.7% molar basis), $CO_2$ capture may be limited by reaction kinetics (as well as mass transfer phenomena) under the conditions investigated. The peak signal intensities assigned to the higher hydrocarbons are observed at a high temperature compared to the permanent gas species and the aldehydes, indicating that these species are evolved via secondary decomposition reactions.

The effect of $CO_2$ capture on the distribution of the product species is presented in terms of the relative ion current intensity data given in Table 4. The presence of CaO has a dramatic influence on the distribution of evolved gas species.

Primarily, the effective capture of $CO_2$ by CaO is demonstrated by a decrease in the relative ion current intensity of $m/z = 44$ by a factor of 8.5 (based on average data for three repeat trials). The enhanced $H_2$ synthesis in the presence of CaO is demonstrated by an increase in the ion current intensity of $m/z = 2$. Furthermore, a significant increase in the relative ion current intensity for $H_2O$ by a factor of 2.6 was observed. This increase in the output of water may be explained by enhanced secondary decomposition reactions. A relative decline in ion current intensity was observed for CO, $CH_4$, higher hydrocarbons, and aldehydes.

To characterize the extent to which the decomposition process is influenced by CaO loading, we conducted experiments with a reduced CaO-to-carbon molar ratio (Ca:C = 0.5). At a reduced sorbent loading there is less sorbent to react with $CO_2$ and $H_2O$, thus both the self-heating and swelling effects are limited. In addition, direct contact between cellulose and sorbent is reduced, potentially limiting the catalytic activity of CaO. The relative ion current intensity data presented in Table 4 clearly indicates a decrease in extent to which $CO_2$ is removed when the loading is reduced. An increase in the relative ion current intensity for $CO_2$ ($m/z = 44$) by a factor of 1.7 shows a direct relationship between sorbent loading and $CO_2$ capture (compared to Ca:C = 1). In addition, an increase in the relative ion current intensities for $m/z = 15$, 26, 27, 28, 29, 30, and 43, and a corresponding decrease for $m/z = 2$ and $m/z = 18$ was observed. A dramatic increase in the final char content from 6.4% wt to 15.6% wt was also observed with the reduced loading. These results demonstrate the important influence of CaO loading on secondary interactions between the evolved species and the decomposing solid. A decrease in the ion current signals assigned to $H_2$ and $H_2O$ suggests a reduction in the secondary decomposition of evolved volatiles. An increase in the char yield may be explained in terms of a decrease in the rate of discharge of volatiles from the decomposing solid due to diminished swelling effects at the reduced CaO loading. Interestingly, no significant change in $T_{peak}$ was observed at the reduced loading. This may be explained if CaO directly catalyses cellulose decomposition via a long-range catalytic mechanism. Clearly further work is required to better elucidate the reaction mechanism.

### *Char formation*

Char formation is influenced by interactions between the evolved gases and the decomposing solids. Final char yields up to 40% wt have been reported during pyrolysis experiments using closed sample holders and evolved water vapor was identified as a catalyst for char formation.[21,24,30] Consistent with these previous studies, in the absence of CaO we observed an increase in char formation (18.9 wt %) using a high ramp rate (100°K/min) and with a sample holder lid.

CaO is expected to enhance the formation of char by catalyzing the tar elimination reactions. The catalytic activity of CaO for tar decomposition leading to the formation of a carbon residue has been reported at high temperatures (i.e. >1073 K).[12,13,37–39] On the other hand, the absorption of $H_2O$ by CaO may undermine the potential catalytic effect of the evolved water vapor. Furthermore, the particle swelling effect due the formation of $Ca(OH)_2$ and $CaCO_3$, which facilitates the escape of evolved gases, may limit gas–solid interactions leading to char formation. Consistent with these competing char formation mechanisms, we observed a maximum char yield of 20.6% with a reduced CaO loading (Ca:C = 0.5 molar basis) and in the presence of additional water vapor. In this case, with a reduced CaO loading, the effects of sorbent hydration, self-heating, and particle swelling were limited.

### *Effect of capping the reaction vessel during heating*

Experiments conducted using a closed reaction vessel provide qualitative insights into the effect of evolved gas residence time and enhanced evolved gas/decomposing solid interactions.

The lid consisted of an alumina disc, which was placed on top of the sample holder. Evolved gases could only escape when the gas pressure inside the closed vessel was sufficient to displace the lid. Thus, the use of the lid is expected to influence the decomposition of cellulose in two key ways. (i) Cellulose decomposition will occur under a higher concentration of evolved gas species, promoting both an increase in the sorbent utilization and evolved gas/decomposing solid interactions; and (ii) evolved gas species spend a longer amount of time at higher partial pressures and temperatures in close proximity to the sample, before dilution with the Ar purge gas. The anticipated effect is an increase in the extent of secondary gas interactions.[28]

Selected thermogravimetric data and relative ion current intensity data is presented in Table 4. In both cases, with and without CaO, we recorded an upwards shift in $T_{peak}$ and a significant reduction in the final char yield at 773 K. These findings are contrary to previous reports in the literature. In fact, Mok et al.[24] reported both an increase in the char yield and a decrease in the $T_{peak}$ for pure cellulose pyrolysis experiments using sealed reaction vessels. The observed decrease in the char yield may be explained on the basis of the relative increase in temperatures of the evolved reactive gases ($H_2O$ and $CO_2$) in close proximity to the sample, favoring the endothermic char gasification reactions.

The relative ion current intensity data for the pure cellulose experiment, both with and without the sample holder lid, is closely comparable, indicating only a minor change in the evolved gas product distribution.

In the case of experiments with CaO, the use of the sample holder lid improved sorbent utilization. This is expected due to the enhanced interaction between the evolved $CO_2$ and CaO. We observed a 29% increase in the utilization of the sorbent from 6.7% without the lid to 8.7% (molar basis) when the lid was used. The relative ion current intensity data (presented in Table 4) demonstrates the effect of superior sorbent utilization on the final product distribution. A decrease in the relative intensity of $m/z = 44$ was recorded and this was accompanied by an increase in the relative intensity of $m/z = 2$. Most dramatic was the increase in the permanent gas yield by factors of 4.5, 1.3, 2.4, and 1.7 for $H_2$, $CH_4$, CO, and $CO_2$ (including $CO_2$ captured), respectively. A corresponding decrease in the amount of evolved water by a factor of 1.2 was observed. An overall increase in the permanent gas yield and the decrease in the $H_2O$ and final char yield indicate the likely catalytic effect of CaO for

catalyzing char gasification reactions. However, we cannot differentiate between the catalytic effect of CaO and the influence of other factors including self-heating. Nevertheless, these results provide qualitative evidence of the significance of the evolved gas residence time for maximizing sorbent utilization.

### *Influence of additional water vapor*

The influence of additional water vapor is expected to significantly effect the decomposition of cellulose and the final distribution of product species. Water vapor has been identified as a catalyst for the char formation mechanism.[21,24] Furthermore, the presence of water vapor is expected to enhance the concentration of $H_2$ according to the water–gas shift reaction Eq. 1, as well as providing an additional driving force for reforming and cracking reactions, according to Eqs. 2, 3, 7, and 8.

To investigate the influence of additional water vapor on the mechanism of cellulose decomposition, water vapor was introduced to the reaction system using a bubbler system (described in "TG-MS"). Thermogravimetric data and the relative ion current intensities for evolved gases from cellulose pyrolysis with additional water vapor (wet gas flow rate = 50 mL/min) are presented in Table 4. Without CaO present, the effect of additional water vapor appears to be only minor. The rate of pyrolysis, represented in terms of $T_{peak}$, is unchanged, and there is no observable enhancement of the char formation mechanism. These observations are consistent with Fushimi et al.[33] who presented matching weight loss profiles for the pyrolysis of cellulose in Ar and in a steam/Ar mixture (Ar:steam = 0.5 molar basis). In addition, no significant changes are observed in the relative ion current data with additional water vapor (Table 4). Similarly, no significant differences were observed when the wet gas flow rate was increased to 100 mL/min (data not shown). To some extent, limited interaction between the decomposing solid and the water vapor and insufficient evolved gas residence time may explain these findings, which are inconsistent with previous literature and equilibrium model predictions. On the basis of a comparison with experiments using the closed reaction vessel, it may be concluded that the influence of evolved gas residence time and specifically evolved gas/decomposing solid interactions (rather than the likely catalytic influence of water vapor) is the dominant factor influencing cellulose decomposition, under the conditions investigated (i.e. without CaO).

When CaO was present, the effect of additional water vapor (wet gas flow rate = 50 mL/min) appeared to exert only a minor influence on the pyrolysis kinetics. In addition, the relative ion current intensity data (Table 4) was similar for cellulose pyrolysis in the presence of CaO, without additional water vapor. Most dramatic was the severe reduction in the final char content (0.7 wt %). This decrease in char formation was matched by a significant increase in the permanent gas yield, i.e. by a factor of 14.4, 5.2, 7.5, and 2.0 for $H_2$, $CH_4$, CO, and $CO_2$ (including $CO_2$ captured). These results suggest that either the char formation mechanism is drastically inhibited under these experimental conditions; alternatively the enhanced permanent gas yield may result from char gasification reactions catalyzed by the presence of

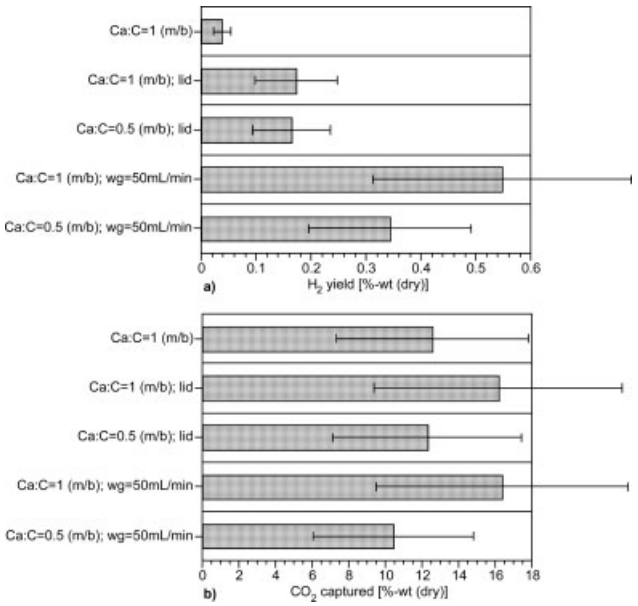


**Figure 8. Influence of the reaction parameters on the total $H_2$ yield (a) and amount of $CO_2$ captured (b).**

The data for $H_2$ yield and $CO_2$ captured is represented as a percentage of the initial dry mass of cellulose (heating rate = 40°K/min). Experimental error was calculated based on variation in the yield of permanent gases, determined for three repeat tests.

CaO. Despite the relatively low temperature (i.e. $T_{peak}$ = 649.6 K) for char gasification, we note that Fushimi et al.[34] reported the formation of a highly reactive char in the presence of water vapor and reported the commencement of char gasification as low as 700 K in the absence of a catalyst. Given the significant increase in the final char content with a reduced CaO loading (20.6% wt), we contend that this likely catalytic effect is short range, and thus limited by direct contact with char. However, in light of the significant variation in final char yield (Table 4), and given the various competing formation mechanisms considered in "Char formation," further work is required to better explain the likely catalytic role of CaO.

### *Maximizing $H_2$ output and $CO_2$ removal*

Figure 8 displays the total $H_2$ yield (a) and $CO_2$ captured (b) for a range of experimental conditions. Our discussion of these quantitative results must be prefaced with an explicit caveat regarding the experimental reproducibility. The error bars displayed in Figure 8 were determined based on three repeat experiments conducted with pure cellulose (heating rate of 40°K/min). We estimated the experimental error based on the standard deviation in the yield data for the detected permanent gases (i.e. $CH_4$, CO, and $CO_2$). Because of the fact that no $H_2$ was detected in these experiments the magnitude of the error bars shown for $H_2$ represents an averaged deviation, expressed as a percentage of the $H_2$ yield.

Despite the uncertainty due to experimental error, these results provide clear insights regarding the effect of key experimental parameters for maximizing $H_2$ synthesis and

effective $CO_2$ capture. The maximum $H_2$ output was recorded for cellulose pyrolysis with CaO (Ca:C = 1 molar basis) and additional water (wet gas flow rate = 50 mL/min). When no water vapor was introduced, we observed a dramatic decline in the $H_2$ yield. The corresponding decline in $CO_2$ removal reflects an overall decline in conversion of cellulose to gas attributable to diminished char gasification reactions. These trends are consistent with thermodynamic modeling predictions and the likely reaction pathways presented in Table 1.

The use of the sample holder lid is shown to enhance both the $H_2$ yield and the amount of $CO_2$ captured, highlighting the importance of the evolved gas residence time and thus improved interaction between the evolved gas and the decomposing solid residue and CaO. A direct relationship between $H_2$ yield and CaO loading is demonstrated by the significant decrease in $H_2$ yield corresponding a decrease in sorbent loading. Interestingly, the decrease in the $H_2$ yield is approximately proportional to the decrease in the amount of $CO_2$ captured.

## Conclusions

Experimental data from a TG-MS study is presented, giving insight into the dominant mechanisms involved in cellulose decomposition in the presence of CaO. Moreover, we have demonstrated the importance of key reaction parameters for maximizing the output of $H_2$. Above all, this study highlights the complexity of the decomposition process, characterized by a host of competing reaction mechanisms, including primary decomposition pathways and secondary interactions governed by the rate of escape of volatile material from the vicinity of the decomposing solid (and subsequent interactions between evolved gas species and the decomposing solid). CaO interacts in this complex reaction system in several ways, via both catalytic and noncatalytic mechanisms. Primarily, CaO was shown to be effective for removing $CO_2$ and a direct trend between the maximum $H_2$ yield and CaO utilization was demonstrated. Additionally, CaO hydration ($Ca(OH)_2$) was shown to be a dominant mechanism. Both of these exothermic gas–solid reactions are predicted by thermodynamic equilibrium theory. The concurrence of these exothermic absorption reactions during cellulose decomposition results in a self-heating effect as well as particle swelling. The self-heating effect is likely to drive secondary decomposition reactions. Particle swelling is thought to facilitate the escape of evolved volatiles from the reaction vessel, thus limiting the char forming reactions. To some extent these effects are inherent to the experimental system used, nonetheless, they clearly highlight the importance of controlling the interactions between the evolved gases and decomposing solid residue for manipulating the distribution of conversion products.

## Acknowledgments

The authors are grateful for the financial support of the Australian Research Council through DP0666488.

## Literature Cited

1. National Renewable Energy Laboratory (NREL). http://www.nrel.gov/biomass/. Accesed on August 21, 2007.
2. Bridgewater AV. The technical and economic feasibility of biomass gasification for power generation. *Fuel*. 1995;74:631–653.
3. Antal MJ Jr, Edwards WE, Friedman HL, Rogers FE. A study of the steam gasification of organic wastes. Technical Report for EPA (EPA-600/7–84-009). *Project Officer Liberick WW Jr*, 1984.
4. Franco C, Pinto F, Gulyurtlu I, Cabrita I. The study of reactions influencing the biomass steam gasification process. *Fuel*. 2003;82:835–842.
5. Higman C, van der Burgt M. *Gasification*. United States of America: Gulf Professional Publishing, 2003.
6. Corella J, Toledo JM, Molina G. Steam gasification of coal at low-medium (600–800°C) temperatures with simultaneous $CO_2$ capture in a fluidized bed at atmospheric pressure: the effect of inorganic species. I. Literature review and comments. *Ind Eng Chem Res*. 2006;45:6137–6146.
7. Turn S, Kinoshita C, Zhang Z, Ishimura D, Zhou J. An experimental investigation of hydrogen production from biomass gasification. *Int J Hydrogen Energy*. 1988;23:641–648.
8. Boateng AA, Walawender WP, Fan LT, Chee CS. Fluidized-bed steam gasification of rice hull. *Bioresour Technol*. 1992;40:235–239.
9. Corella J, Aznar MP, Delgado J, Aldea E. Steam gasification of cellulosic wastes in a fluidized bed with downstream vessels. *Ind Eng Chem Res*. 1991;30:2252–2262.
10. Herguido J, Corella J, Gonzalez-Saiz J. Steam gasification of lignocellulosic residues in a fluidized bed at small pilot scale. Effect of type of feedstock. *Ind Eng Chem Res*. 1992;31:1274–1282.
11. Walawender WP, Hoveland DA, Fan LT. Steam gasification of pure cellulose. I. Uniform temperature profile. *Ind Eng Chem Process Des Dev*. 1985;24:813–817.
12. Simell PA, Leppalahti JK, Bredenberg BS. Catalytic purification of tarry fuel gas with carbonate rocks and ferrous materials. *Fuel*. 1992;71:211–218.
13. Simell PA, Leppalahti JK, Kurkela EA. Tar-decomposing activity of carbonate rocks under high $CO_2$ partial pressure. *Fuel*. 1995;74:938–945.
14. Sakadjian BB, Iyer MV, Gupta H, Fan L-S. Kinetics and structural characterisation of calcium-based sorbents calcined under subatmospheric conditions for the high-temperature $CO_2$ capture process. *Ind Chem Res*. 2007;46:35–42.
15. Corella J, Toledo JM, Molina G. A review on dual fluidized bed biomass gasifiers. In Preprint from Proceedings of the 15th European Biomass Conference, 7–11 May, Berlin, Germany, 2007.
16. Pfeifer C, Puchner B, Hofbauer H. In-situ $CO_2$-absorption in a dual fluidised bed biomass steam gasifier to produce a hydrogen rich syngas. *Int J Chem Reactor Eng*. 2007;5:A9.
17. Pfeifer C, Puchner B, Proll T, Hofbauer H. $H_2$-rich syngas from renewable sources by dual fluidized bed steam gasification of solid biomass. In ECI Conference, The 12th International Conference on Fluidization, New Horizons in Fluidization Engineering, Vancouver, Canada, 2007.
18. Florin NH, Harris AT. Hydrogen production from biomass coupled with carbon dioxide capture: the implications of thermodynamic equilibrium. *Int J Hydrogen Energy*. 2007;32:4119–4134.
19. Hanaoka T, Inoue S, Uno S, Ogi T, Minowa T. Effect of woody biomass components on air-steam gasification. *Biomass and Bioenergy*. 2005;28:69–76.
20. Hanaoka T, Yoshida T, Fujimoto S, Kamei K, Harada M, Suzuki Y, Hatano H, Yokoyama S-Y, Minowa T. Hydrogen production from woody biomass by steam gasification using a $CO_2$ sorbent. *Biomass and Bioenergy*. 2005;28:63–68.
21. Antal MJ Jr, Varhegyi G. Cellulose pyrolysis kinetics: the current state of knowledge. *Ind Eng Chem Res*. 1995;34:730–717.
22. Evens RJ, Milne TA. Molecular characterisation of the pyrolysis of biomass. I. *Fundam Energy Fuels*. 1987;1:123–137.
23. Gronli M, Antal MJ Jr, Varhegyi G. A round-robin study of cellulose pyrolysis kinetics by thermogravimetry. *Ind Eng Chem Res*. 1999;38:2238–2244.
24. Mok WS-L, Antal MJ Jr, Szabo P, Varhegyi G, Zelei B. Formation of charcoal from biomass in a sealed reactor. *Ind Eng Chem Res*. 1992;31:1162–1166.
25. Richards GN. Glycoaldehyde from pyrolysis of cellulose. *J Anal Appl Pyrolysis*. 1987;10:251–255.

26. Richards GN, Zheng G. Influence of metal ions and of salts on products from pyrolysis of wood: applications to the thermalchemical processing of newsprint and biomass. *J Anal Appl Pyrolysis*. 1991; 21:133–146.
27. Shafizadeh F. Introduction to pyrolysis of biomass. *J Anal Appl Pyrolysis*. 1982;3:283–305.
28. Varhegyi G, Antal MJ Jr, Szekely T, Till F, Jakab E. Simultaneous thermogravimetric-mass spectrometric studies of the thermal decomposition of biopolymers. I. Avicel cellulose in the presence and absence of catalysts. *Energy and Fuels*. 1988;2:267–272.
29. Varhegyi G, Antal MJ Jr, Szekely T, Till F, Jakab E, Szabo P. Simultaneous thermogravimetric-mass spectrometric studies of the thermal decomposition of biopolymers. II. Sugar cane bagasse in the presence and absence of catalysts. *Energy and Fuels*. 1988;2:273–277.
30. Varhegyi G, Szabo P, Mok WSL, Antal MJ Jr. Kinetics of the thermal decomposition of cellulose in sealed vessels at elevated pressures. Effects of the presence of water on the reaction mechanism. *J Anal Appl Pyrolysis*. 1993;26:159–174.
31. Varhegyi G, Antal MJ Jr, Jakab E, Szabo P. Kinetic modeling of biomass pyrolysis. *J Anal Appl Pyrolysis*. 1997;42:73–87.
32. Piskorz J, Radlein DAG St, Scott DS, Czernik S. Pretreatment of wood and cellulose from the production of sugars by fast pyrolysis. *J Anal Appl Pyrolysis*. 1989;16:127–142.
33. Fushimi C, Araki K, Yamaguchi Y, Tsutsumi A. Effect of heating rate on steam gasification of biomass. I. Reactivity of char. *Ind Eng Chem Res*. 2003;42:3922–3928.
34. Fushimi C, Araki K, Yamaguchi Y, Tsutsumi A. Effect of heating rate on steam gasification of biomass. II. Thermogravimetric-mass spectrometric (TG-MS) analysis of gas evolution. *Ind Eng Chem Res*. 2003;42:3929–3936.
35. Davis R, Frearson M. *Mass Spectrometry—Analytical Chemistry by Open Learning*. Pritchard EF on behalf of ACOL. Wiley, 1987.
36. Borgwardt RH. Sintering of nascent calcium oxide. *Chem Eng Sci*. 1989;44:53–60.
37. Abu El-Rub Z, Bramer AE, Brem G. Review of catalysts for tar elimination in biomass gasification. *Ind Eng Chem Res*. 2004;43: 6911–6919.
38. Delgado J, Aznar MP, Corella J. Biomass gasification with steam in fluidized bed: effectiveness of CaO, MgO and CaO-MgO for hot raw gas cleaning. *Ind Eng Chem Res*. 1997;36:1535–1543.
39. Delgado J, Aznar MP, Corella J. Calcined dolomite, magnesite and calcite for cleaning hot gas from a fluidised bed biomass gasifier with steam: life and usefulness. *Ind Eng Chem Res*. 1996;35:3637–3643.

*Manuscript received Aug. 30, 2007, and revision received Dec. 3, 2007*